HHS Public Access

Author manuscript

IEEE Trans Neural Syst Rehabil Eng. Author manuscript; available in PMC 2016 January 01.

Published in final edited form as:

IEEE Trans Neural Syst Rehabil Eng. 2015 January ; 23(1): 116–127. doi:10.1109/TNSRE.2014.2348415.

Suppression of Subthalamic Nucleus Activity by Micromagnetic Stimulation

Seung Woo Lee and

Massachusetts General Hospital, Department of Neuro-surgery, Harvard Medical School, Boston, MA 02114 USA (Lee.Seungwoo@mgh.harvard.edu).

Shelley I. Fried

Boston Veterans Administration Healthcare System, Rehabilitation, Research and Development, Boston, MA 01230 USA and also with Massachusetts General Hospital, Department of Neurosurgery, Harvard Medical School, Boston, MA 02114 USA (Fried.Shelley@mgh.harvard.edu).

Abstract

Magnetic stimulation delivered via 0.5-mm diameter coils was recently shown to activate retinal neurons; the small coil size raises the possibility that micromagnetic stimulation (μMS) could underlie a new generation of implanted neural prosthetics. Such an approach has several inherent advantages over conventional electric stimulation, including the potential for selective activation of neuronal targets as well as less susceptibility to inflamma-tory responses. The viability of μMS for some applications, e.g., deep brain stimulation (DBS), may require suppression (rather than creation) of neuronal activity, however, and therefore we explore here whether (μMS) could, in fact, suppress activity. While single pulses elicited weak and inconsistent spiking in neurons of the mouse subthalamic nucleus (*in vitro*), repetitive stimulation effectively suppressed activity in ~70% of targeted neurons. This is the same percentage suppressed by conventional electric stimulation; with both modalities, suppression occurred only after an initial increase in spiking. The latency to the onset of suppression was inversely correlated to the energy of the stimulus waveform: larger amplitudes and lower frequencies had the fastest onset of suppression. These findings continue to support the viability of μMS as a next-generation implantable neural prosthetic.

Keywords

Deep brain stimulation (DBS); magnetic stimulation; neural prosthesis; Parkinson's disease (PD); repetitive transcranial magnetic stimulation (rTMS); subthalamic nucleus (STN)

I. Introduction

THE use of electric stimulation to alleviate disorders of the neural system is well established. For example, deep brain stimulation (DBS) effectively reduces the symptoms

associated with diseases such as Parkinson's Disease, essential tremor and dystonia [1]–[3]. Cochlear prosthetics have also proven effective in restoring the sensation of hearing to patients that are profoundly deaf [4], [5]. Success with these types of devices has prompted the evaluation of a wide range of new approaches including visual prosthetics [6]–[10] (retinal and cortical), several types of limb prosthetics [11], [12] as well as many new DBS treatments for neural disorders including Tourette's Syndrome [13], obsessive-compulsive disorder [14], [15], chronic pain [16], depression [17] and epilepsy [18].

Despite these successes there are several fundamental limitations associated with the use of conventional electric stimulation. For example, although it is often desirable to confine the effects of stimulation to a small region, i.e., within a specific nucleus, it is often difficult to prevent the spread of activation, e.g., the activation that arises when passing axons from nontargeted regions become activated. The activation of such regions can lead to a wide array of problematic side effects [2], [19]–[22]. A second limitation arises from the inflammatory reactions generated in response to implantation. These reactions can lead to scarring around the electrode that can alter the performance of the device over time, i.e., increasing the thresholds for activation [23]–[29].

Magnetic stimulation is another well-established approach for modulating neuronal activity. For example, transcranial magnetic stimulation (TMS) utilizes large coils positioned adjacent to the scalp to modulate activity of cortical neurons [30]. TMS has demonstrated moderate success for the clinical treatment of some forms of depression [31] and is currently under evaluation for other neurological and psychiatric disorders (e.g., migraine headaches, strokes, and tinnitus) [32]–[35]. It has not been successful however for targeting deeper targets, e.g., neurons of the basal ganglia, probably because of the rapid fall-off of magnetic field strength with distance. Unfortunately, the large size of TMS coils prohibits implantation and until recently, the possibility of implanting smaller coils into the parenchyma was not considered viable because the fields induced by small coils were thought to be not strong enough to modulate neuronal activity. However, several recent studies have found that small coils [36], [37], including ones as small as 0.5 mm in diameter [36], could in fact activate neurons. Because such coils are small enough to be implanted, these findings raise the possibility that micromagnetic stimulation (μMS) could form the basis of one or more next-generation neural prosthetic devices.

Magnetic stimulation has some intriguing potential advantages over conventional electric stimulation. One such advantage is that the electric fields induced by coils are spatially asymmetric and may therefore allow focal targeting of specific regions around the coil. For example, Bonmassar *et al.* [36] showed that the induced electric fields along the length of the coil were approximately 10× stronger than the fields along the two (circular) end plates. As such, it is likely that neurons along the length of the coil would be preferentially activated versus neurons closer to the coil edges. Consistent with the modeling results, Bonmassar *et al.* showed that selective populations of retinal neurons could be activated by some orientations of the coil but not by others. One particularly attractive finding was that the passing axons that run along the inner retinal surface could be avoided when the orientation of the coil was such that the induced electric fields were oriented perpendicularly to the surface, e.g., the gradient of field along the axon was low [38], [39]. Another potential

advantage of μMS over conventional electric stimulation arises from the fact that μMS coils can be coated with a bio-inert polymer, e.g., parylene [40], polyimide [41], [42], and liquid crystal polymers [42]–[44], without any appreciable loss of efficacy; the lack of direct contact between the metal electrode and neural tissue may reduce the inflammatory response associated with implantation. Further, because magnetic fields pass readily through a wide range of biological tissue, e.g., blood, bone, etc., the formation of any sort of glial scar surrounding the implant would likely have little or no influence on the activation of targeted tissue, i.e., thresholds would not increase over time. While scarring and threshold increases are not as problematic for large electrodes, i.e., those used in DBS, thresholds can increase significantly for smaller microelectrodes [29].

Before μMS can be fully considered as an alternative to conventional implanted electric stimulation devices, however, it is necessary to better understand its capabilities and limitations, especially as related to its ability to modulate neuronal activity. The retina contains many structural and functional differences from other regions of the CNS and as such, significant differences in sensitivity to μMS may exist. In addition, while the excitatory effects in the retina arose from single pulses, previous studies have found that both excitatory and inhibitory effects can be elicited by varying the rate at which magnetic stimulation is delivered [33]. Along similar lines, previous *in vitro* experiments showed that neurons of the subthalamic nucleus (STN) were suppressed by high-rate stimulation (after an initial transient burst of activity) [45]–[47]. While this previous inhibitory effect may be restricted to only certain parts of the neuron [48], it is nevertheless important to understand whether μMS can suppress or otherwise alter neural activity (in addition to the excita-tory effects shown previously) before an informed decision can be made about its suitability for applications such as DBS.

One additional consideration of great practical importance for μMS concerns the power required for use. Previous (unpublished) work from our lab found that power levels required for activation of retinal neurons was 12.4 mJ per (single) pulse of μMS. Of this energy, 0.78 mJ was associated with the initial short-duration bi-phasic pulse and 11.64 mJ was associated with the subsequent damped sinusoid [cf. Fig. 2(b)]. Unfortunately, it is not known which of the two components underlie neuronal activation (both could also contribute). However, even if activation was mediated by only the short bi-phasic component, the power required to generated such pulses at 150 Hz (~ 120 mJ) will greatly exceed even the upper limit of the power range used by existing devices (e.g., the Medtronic DBS Model 37601 Activa PC neurostimulator: 1.54 mJ @ 3.5 V, 210 μs, and 150 Hz) [49]. Higher power levels will necessitate more frequent changes of the implanted power supply with a corresponding increase in the number of surgical procedures and al most certainly an increase in the number of surgical complications [1]. Thus, the ability to bring the power levels associated with μMS more in line with those from existing neural prosthetics, or perhaps even reduce the power to levels below that of existing devices would be highly desirable.

Here, we studied the response of STN neurons *in vitro* to μMS. Responses to single pulses were generally weak and/or required high thresholds for activation and therefore, we examined whether delivery of trains of pulses might be more effective. However, because

the amplifier distorted the shape of the pulse waveform we switched to sinusoidal waveforms and studied the effect of trains of sinusoids, e.g., ten cycles of a 500 Hz waveform. Surprisingly, we found that the effects of such trains were in fact strongly suppressive if they were delivered over a long period of time. Finally, we studied how changes to the parameters of the sinusoidal train influenced the suppressive effect. Our results support the notion that μMS may one day be a suitable alternative to conventional electric stimulation based devices.

II. Methods

A. Preparation and Testing of μMS Coils

We purchased commercial multilayer inductors (ELJRFR10JFB, Panasonic Electronic Devices Corporation of America, Knoxville, TN) and soldered (15-mils 44-resin core SN63PB37) (Kester, Itasca, IL) the two leads to copper wire (34-AWG, polyurethane inner coat and nylon over coat) (Belden, Richmond, IN). Assembled coils were coated with 10-μm-thick parylene-C coating (EIC Laboratories, Norwood, MA, USA) to eliminate the possibility that responses were mediated by a leakage of current from the coil assembly into the slice preparation. After coating, the coil was placed on the tip of a custom-made plastic tube 300 mm long; and the distal ends were attached to the signal and ground leads of a BNC connector. The custom-made tube was fabricated from a disposable plastic pipette (BD Falcon Serological Pipet; 5 ml in 1/10 ml; BD Biosciences, San Jose, CA) by cutting the end to be 300 mm in length so that the coil assembly could be secured to the micromanipulator for positioning near the mouse brain slice.

Because the outer boundaries of the coil as well as the parylene-C coating were discernible under the microscope with the IR illumination system used during *in vitro* experiments, it was possible to position the coated coil above the STN area in x-y plane. However, the coil was opaque to the IR illumination and so it was necessary to perform preliminary measurements [36] to reveal the distance in z-direction between the coil outer boundary and the brain slice. The bottom edge of the coated coil was determined relative to a focal point at or near the top surface of the assembly so that the height of the coil above the brain slice could be reasonably estimated. In this manner, the distance from the brain preparation to the closest edge of the coil (inside coating) could be reliably controlled and was set to ~ 300 μm in all experiments.

The μMS coil assemblies were tested before and after each experiment to ensure that there was no leakage of current. If present, such currents could have contributed to the observed neural activity. The coils were submerged in physiological solution (0.9% NaCl) and the impedance between one of the coil terminals and an electrode immersed in the physiological solution was measured before and after each electrophysiological experiment. Impedances above 200 MΩ were considered indicative of adequate insulation.

In a few experiments, it was necessary to create a gap in the coil so as to electrically isolate the two ends. This was accomplished by passing high levels of current through the coil (3 A) for ~ 10 ms. A break in the coil was detected by measuring the impedance across the coil: impedances increased from 7-8 Ω in the intact coil to > 200 MΩ after the break. The

impedance between both ends of the coil and the bath was also confirmed to be > 200 MΩ so as to ensure that the insulation surrounding the coil had not burned (i.e., there was no direct path for electrical current into the bath).

B. *μ*MS *Drive*

The output of a function generator (AFG3021B, Tektronix Inc., Beaverton, OR) was connected to a 1000 W audio amplifier (PB717X, Pyramid Inc., Brooklyn, NY) with a bandwidth of 70 kHz. Pulsatile coil input had amplitudes ranging from 0–10 V in steps of 0.5 V and durations ranged from 20 *μ*s – 1 s. The rate of increase of the leading edge was 18 ns/V; the decrease of the trailing edge was at an equal rate. The output of the amplifier for the pulsatile input consisted of a sharp peak at both the leading and trailing edges of the pulse followed by a damped cosine waveform (monitored with a TDS2014C oscilloscope, Tektronix Inc., Beaverton, OR). The peak had maximum amplitudes ranging from 0–28.7 V (gain of 2.87 V/V) with leading/trailing edge slopes of 80 ns/V. The duration of each peak was ~ 20 *μ*s and the two peaks were separated by 500 *μ*s (the duration of the pulse). The amplitude of the damped sinusoid was smaller than the amplitude of the peak and ranged from 0–10 V; its duration was approximately 12 ms. Sinusoid coil input had a fixed amplitude of 1.5 V and frequencies ranged from 250–1000 Hz. The output of the amplifier for the sinusoid input was linearly amplified to 4.3 V (2.87 V/V).

C. Animal Preparation and Brain Slice Preparation

Electrophysiological recordings were performed using brain slices prepared from 17–30 days old mice (C57BL/6J; Jackson Laboratory, Bar Harbor, ME). The care and use of animals followed all federal and institutional guidelines, and the Institutional Animal Care and Use Committees of the Boston VA Healthcare System and the Subcommittee of Research Animal Care of the Massachusetts General Hospital. The mice were deeply anesthetized with isoflurane and decapitated. The brains were removed immediately after death and a section of the brain containing the STN was isolated on ice in a 0–5°C oxygenated solution containing (in mM) 1.25 NaH2PO4, 2.5 KCl, 25 NaHCO3, 1 MgCl2, 25 glucose, and 225 sucrose, equilibrated with 95% O2–5% CO2 (pH 7.4). This cold solution, with a low sodium ion and without calcium ion content, improved tissue viability. In the same medium, 300–400 *μ*m thick coronal slices were prepared using a vibrating blade microtome (Vibratome 3000 Plus, Ted Pella, Inc., Redding, CA) and were incubated at room temperature in an artificial cerebrospinal fluid (aCSF) solution containing (in mM) 125 NaCl, 1.25 NaH2PO4, 2.5 KCl, 25 NaHCO3, 1 MgCl2, 2 CaCl2, and 25 glucose, equilibrated with 95% O2–5% CO2 (pH 7.4). After a two hour recovery period, STN slices were transferred and mounted, caudal side down, to a plastic recording chamber (RC-27L, Warner Instruments, LLC, Hamden, CT) with plastic slice anchor (SHD-27LP/2, Warner Instruments). The chamber with slices was maintained at 30 ± 2°C, and continuously superfused (3 ml/min) with oxygenated aCSF solution.

D. Electrophysiology

Patch pipettes were used to make small holes on the surface of brain slice, and STN neurons were targeted under visual control. Spiking was recorded with a patch electrode (4–8 MΩ)

that was filled with superfusate and positioned onto the surface of a targeted ganglion cell (cell-attached mode). Two silver-chlo-ride-coated wires served as the ground and were positioned at opposite edges of the recording chamber, each approximately 15 mm from the targeted cell. Recording of spontaneous spiking for 60 seconds was used to determine whether an appropriate patch seal had been established and also to confirm that the cell was functioning normally; only those cells that generated spontaneous spiking were tested with μMS. The μMS coil assembly was fixed in the micromanipulator such that the main axis of the coil was oriented parallel to the brain slice surface (Fig. 1). The coil assembly was lowered into the bath until the coil was 300 μm above the brain slice surface.

E. Data Analysis

Raw waveforms were recorded at a sample rate of 100 kHz and processed with custom software written in MATLAB. Each elicited waveform contained an electrical artifact arising from the pulsatile or sinusoid μMS; the pulsatile μMS artifact lasted ~ 20 ms and was nearly identical for trials with identical stimulus conditions; the sinusoid μMS artifact did not show the prolonged artifact and was readily removed by using the notch filter for the specific frequencies in MATLAB. Many elicited responses also contained a series of action potentials (spikes); these were confirmed as spikes by comparing them to those spikes elicited spontaneously (Section III). The timing of individual spikes was determined with a "matched filter" – the average spontaneous spike was cross-correlated with the response waveform; peaks in the cross correlation were used to assign timing of individual action potentials [50]–[52].

III. Results

We ran a series of electrophysiological experiments using coronal slices from the mouse brain to explore whether neurons of the subthalamic nucleus (STN) could be modulated by micro-magnetic stimulation (μMS) from a small coil (Section II). The microcoil was positioned ~ 300 μm above the surface of the slice and centered approximately over the STN [Fig. 1(a)]; the coil was oriented such that its long axis was parallel to the surface of the slice [Fig. 1(b)] and also approximately parallel to the "long axis" of the STN [dotted lines in Fig. 1(a)]. A patch clamp electrode was positioned on the soma of a targeted STN neuron in the cell-attached configuration in order to detect action potentials (APs). Recordings were typically started approximately 60 s prior to the onset of stimulation in order to confirm viability of the recording system as well as to determine the pattern of spontaneous APs; only those cells that generated spontaneous APs were subjected to further study. The results below are derived from recordings in 43 cells (17 different slices).

A monophasic rectangular pulse with duration of 500 μs [Fig. 2(a)] was input to the amplifier—the output waveform from the amplifier is shown in Fig. 2(b) and consists of a short duration (~ 20 μs) bi-phasic waveform [Fig. 2(b)]; inset: negative and positive peaks occurred at the leading and trailing edges of the pulse (respectively) and were separated by a 500-μs interval) and followed by a damped sinusoidal waveform that had a period of ~ 4 ms (Section II); this was the waveform delivered to the coil. The measured response to this stimulus similarly consisted of a short duration bi-phasic waveform followed by a more

prolonged damped sinusoid [Fig. 2(c)]. The damped sinusoid portion of the artifact was typically relatively smooth [Fig. 2(c), dashed line] but sometimes contained an additional multiphasic waveform (horizontal arrow) that occurred with a latency of ~ 1 ms [Fig. 2(c), solid line]. Subtraction of the two waveforms (inset) revealed a waveform that had nearly identical amplitude and kinetics to action potentials that arose spontaneously suggesting it too was an AP. The submillisecond latency of this elicited action potential suggests that it arose from direct activation of the STN neuron, i.e., not secondary to activation of one or more presynaptic neurons. We were only able to elicit action potentials in this manner for three of seven cells in which pulsatile stimulation was delivered. Further, the pulse amplitude required to elicit action potentials in these three cells was high (23 V). Previous estimates of the strength of the induced electric field arising from this coil were ~ 80 V/m, greater than the field strength thought to be necessary to modulate neuronal activity [53] making it somewhat curious that cells did not respond more consistently. We also did not observe burst firing (two or more spikes) for all cells tested with pulsatile stimulation (n = 7).

Because the thresholds required for activation of STN neurons with single pulses were close to the upper limit of our stimulation system, we questioned whether activation could be achieved more consistently via repetitive stimulation at lower amplitudes. We were not sure of the time scale over which temporal integration might occur and therefore were concerned about the prolonged nature of the electric artifact, especially the damped sinusoidal portion. To address this concern we changed the stimulus waveform from pulsatile to sinusoidal; since sinusoids passed through our amplifier without distortion this would allow the interval between successive stimuli to be more precisely regulated. Although sinusoids have a smaller di/dt than do pulses (and therefore a correspondingly smaller B and E) [36], we reasoned that the presentation of repetitive subthreshold effects, even if they were somewhat reduced, might nevertheless summate and lead to spiking. Consistent with this notion, high-rate stimulation has previously been shown to effectively modulate neuronal activity [50].

As a first step, we ran a series of experiments to explore whether 500-Hz sinusoidal stimulation would activate STN neurons (Fig. 3). Ten cycles of the 500-Hz sinusoid were presented consecutively at one-second intervals (repetition rate of 1 Hz) [Fig. 3(a)]. Several typical one-second response periods are shown in Fig. 3(b). The artifact in response to the stimulus is indicated by the arrow at the start of the first trial. Several spikes were typically observed in the one-second window following each stimulus. However, the timing of such spikes was not consistent from trial to trial suggesting that observed spikes might simply reflect normal baseline spiking. To further explore this, we created raster plots that included 50 one-second intervals prior to the onset of stimulation [Fig. 3(c)], below horizontal line) as well as 50 one-second intervals each following a μMS stimulus [Fig. 3(c)], above horizontal line). The level of spiking within the rasters appeared similar from before and after the onset of stimulation as were the corresponding peri-stimulus time histograms (PSTHs) [Fig. 3(d)]. As a final comparison, we calculated the total number of spikes elicited over time for both pre and post stimulus time windows [Fig. 3(e)]. In some cases, there were slightly more total spikes for post-stimulus than for pre-stimulus (left panel). However, there was some variability across the population and some cells generated less spikes post-stimulus (middle

panel). We averaged the responses across all cells and found that on average there was a slight increase to the number of spikes post-stimulation (versus pre-stimulation) [Fig. 3(e), right panel]. In no cases (n = 28) did we observe elicited spikes that were phase locked to the μMS stimulus. The fact that the spike totals following the onset of μMS were not linear over time [i.e., there were slight inflection points in the curves of Fig. 3(e)], raised the possibility that even longer trains of stimulation (> 50 s) might reveal additional changes.

Interestingly, prolonged stimulation using ten periods of 500-Hz sinusoids delivered at 1 Hz had a suppressive effect on most STN neurons. Responses from a typical cell are shown in raster form in Fig. 4(a) (top); the corresponding PSTH is shown in Fig. 4(a) (bottom). Expanded one-second windows of the raw trace at different time points are shown in the panels of Fig. 4(b). Prior to the onset of stimulation [Fig. 4(b), Panel 1], the cell exhibited a modest level of baseline activity. There was no immediate change in the cell's response to stimulation but after ~1–2 minutes of continuous stimulation, the cell exhibited a significant increase in the rate of spiking (Panel 2). The increased spiking persisted from 8–90 seconds (mean 50 ± 27 s; n = 17) but eventually, the pattern of increased spiking began to look irregular (Panel 3). Shortly afterwards spiking subsided completely (Panel 4) and the cell remained quiet for the duration of the stimulus (Panel 4). Within a minute after termination of the stimulus, spiking resumed in the cell (Panel 5), often with a transient surge in the spike rate. Although there was some variability in several aspects of the response [Fig. 4(c), left and right panels], qualitatively similar response patterns were observed in 21/28 cells for which this stimulus was tested. It is interesting to note that the patterns observed here (transient increase in spike rate followed by silencing) are highly similar to the patterns observed in response to electric stimulation of STN neurons *in vitro* [45]–[47]. Further, the percentage of cells suppressed here by μMS (75%) is nearly identical to the percentage reported in the electric stimulation studies (68% in Margarinos-Ascone *et al.* [46]). Although neither our work nor the Margarinos-Ascone *et al.* study identify the mechanism by which spiking suppression occurs, the fact that response patterns were similar and also occurred in a similar percentage of cells raises the possibility that whatever the mechanism, it was similar for both types of stimulation.

There was some variability in the responses from STN neurons that were not silenced by μMS (n = 5/28, Fig. 5). Some exhibited a maintained increase in firing rate (n = 2) [Fig. 5(a)] while others (n = 3) exhibited only a transient increase [Fig. 5(b), top and bottom panels from two different cells]. In still other cells (n = 2/28) [Fig. 5(c)], spiking persisted but appeared burst-like. The distinguishing feature of all these cells was that spiking persisted throughout the course of stimulation, at least for the 7 minutes of stimulation during which it was observed. A breakdown of the different responses is shown in Fig. 5(d).

The reasons for the different response patterns were not revealed by the experiments performed in this study but interestingly, the kinetics of action potentials changed for some response classes but not for others (Fig. 6). The most notable change occurred during the course of stimulation for those cells that were silenced by μMS [Fig. 6(a)]. The duration of the depolarizing phase of a typical action potential prior to the onset of stimulation was ~ 0.5 ms [Fig. 6(a), solid thin black]. Just prior to the suppression of spiking, when the firing rate was near maximum, the duration of the depolarization phase increased to ~ 2 ms [Fig. 6(a),

solid thick gray]. After the cessation of μMS and the reinitiation of spiking, the kinetics of spontaneously arising action potentials returned almost identically to control [Fig. 6(a), thin dashed]. For those cells that were not suppressed by μMS [Fig. 5(a), (b)], there was no broadening of the depolarizing phase and the overall kinetics remained highly similar [Fig. 6(b)]. For the few cells that responded to prolonged μMS with burst-like spiking [Fig. 5(c)], we observed a broadening of the depolarizing phase of the action potential, similar to that shown for cells that were silenced [Fig. 6(a)]. However, these few cells did not exhibit a further decline in the action potential kinetics and the altered spike waveform persisted for the duration of μMS (not shown).

To explore how the parameters of stimulation influenced the silencing of STN neurons, we measured the duration from the onset of stimulation to the point at which spiking was completely suppressed (referred to as “time-to-silence”) for several different parameter sets. For example, to determine how the rate at which μMS was delivered influenced silencing, one cycle of 500-Hz sinusoidal coil was delivered at repetition rates of 1, 10 and 50 Hz [Fig. 7(a)]. The average time-to-silence of STN neurons decreased as the repetition rate increased [Fig. 7(b)] suggesting that higher rates of μMS stimulation had a stronger suppressive effect. A similar effect was observed when changing the waveform frequency: one cycle of a 1000, 500 or 250 Hz sinusoid was delivered at a constant repetition rate of 50 Hz [Fig. 7(c)]. The average time to silencing decreased as the period of the input waveform increased [Fig. 7(d)] again suggesting that higher levels of μMS are more effective in suppressing spiking. In a final set of experiments, we compared the effects when the total level of μMS energy delivered was held constant over a fixed period of time but the temporal distribution within that time period was varied [Fig. 7(e)]. Specifically, the total number of stimulation periods was held constant during one-second periods (ten total cycles per second) but the rate at which the ten cycles were delivered was varied: in one case, all ten cycles were delivered at the start of the one-second period [Fig. 7(e), top row]. In another case, two cycles were delivered every 200 ms (middle row) while in the final case, a single cycle was delivered every 100 ms (bottom row). Interestingly, the time-to-silence was shortest when the ten cycles were spread out over the course of the one second interval [Fig. 7(f)].

We estimated the power associated with the different forms of μMS delivery tested here. For pulsatile stimulation, the average voltage at threshold was 23.0 V and the average current at threshold was 2.88 A (the dc impedance of the coil, 8 Ω, was assumed constant at the low frequencies used here). Because this level occurred only at the peak of the bi-phasic waveform [e.g., Fig. 2(b)], integration was needed to find the areas under each portion of the curve (bi-phasic and damped sinusoid). In this manner, the power estimates were 1.32 mJ for the bi-phasic component and 38.48 mJ for the damped sinusoid. These values are for a single pulse; stimulation at higher rates would yield proportionately higher values. For sinusoidal stimulation at 500 Hz, the voltage used here was 4.3 V which corresponded to a current of 0.538 A and a power level per period of 2.31 mJ. A single period at 1000 Hz had a power level of 1.16 mJ.

Estimates of the strength of the electric field arising from 500 Hz sinusoids were 0.2–0.3 V/m; well below the field strength associated with pulsatile stimulation but comparable to field strengths shown previously to be effective for modulation of hippocampal neurons

[54]. Since field levels were small we thought it prudent to consider the possibility that nonmagnetic factors might be contributing to the observed responses. Power to the coil was supplied via a battery and therefore there was no electrical coupling between the coil and the bath ground. As such, capacitive current was not forced through the tissue as in previous work [55], suggesting that activation was not mediated by a capacitive effect. To further confirm this, we induced a break in the coil by passing strong electrical current (Section II); the break resulted in a change in impedance across the coil from ~ 8 Ω to > 200 MΩ effectively isolating the two end plates and thereby allowing each to maintain a separate voltage, i.e., act as a capacitor. When stimulation was delivered through the broken coil there was no indication of neuronal modulation (n = 5) allowing us to conclude that the observed neuronal responses were not mediated by a capacitive effect. The possibility of direct electrical activation was also eliminated by ongoing verification of the integrity of the coil insulation (Section II).

To rule out possibilities such as thermal shock or inadvertent inductances, i.e., those arising from the circuitry supplying the coil, it was necessary to change preparations to coronal slices of the mouse prefrontal cortex (PFC). We targeted layer 5/6 pyramidal neurons as such neurons have their long-axis within the plane of the slice enabling a direct comparison of two different coil orientations (Fig. 8) (the axons of STN neurons project downwards into the slice). One orientation was such that the coil axis was perpendicular to the long axis of the targeted pyramidal cell [“parallel orientation”, Fig. 8(a)] while in the other case the long axis of the coil was parallel to and directly above the long axis of the cell [“perpendicular orientation”, Fig. 8(c)]. In both cases, the long-axis of the coil remained parallel to the slice surface with its bottom edge fixed at a distance of 100 μm above the slice surface. Regardless of orientation, the center of the coil remained fixed over the apical dendrite at a location ~ 200 μm from the soma.

Under control conditions, pyramidal cells are mostly unresponsive to electric stimulation and were similarly unresponsive to single pulses of magnetic stimulation regardless of the orientation of the coil (not shown). Repetitive stimulation, consisting of 10-Hz stimulation for a period of 2–3 minutes was similarly ineffective when the coil was in the perpendicular orientation [Fig. 8(d)] but elicited spiking when the coil was rotated to the parallel orientation [Fig. 8(b)]. Once the cell began firing, it was generally more responsive to stimulation, e.g., responses to repetitive stimulation (parallel orientation) occurred within one second (not shown). Despite the increased level of responsiveness, only the parallel orientation of the coil remained effective, responses were never elicited when the coil was in the perpendicular orientation.

Because one orientation of the coil was effective and the other orientation of the same coil was not, we could eliminate the remaining nonmagnetic mechanisms of activation. For example, if activation were in fact arising from some sort of thermal shock induced by heating of the coil, the closer alignment of the coil to the cell in the perpendicular configuration should have been more effective. Instead, the perpendicular orientation was completely ineffective while the parallel orientation elicited a strong effect. The experiments of Fig. 8 also eliminate the possibility that activation arose from inductances associated with the supply circuitry as responses were different even though the circuitry was identical for

the two coil orientations. We monitored the integrity of the coil insulation in these experiments as well thereby eliminating the possibility of direct electrical activation. Thus, our control experiments eliminate the possibility that activation arose from: 1) direct electrical effects via a leakage current; 2) a capacitive effect; 3) thermal shock; or 4) stray inductances and we therefore conclude that activation does in fact arise from the electric fields induced by flow of current through the small coils.

IV. Discussion

The effectiveness of single pulses of μMS for the activation of STN neurons was quite limited. This is in contrast to previous work in which μMS reliably elicited spiking in retinal ganglion cells. For example, single short pulses of μMS in the retinal study each elicited a burst of action potentials (latency of spiking onset was ~ 50 ms) when the central axis of the coil was aligned parallel to the retinal surface. Much previous work with electric stimulation of the retina [6], [51], [52], [56], [57] indicates that burst firing arises secondary to the activation of bipolar cells, a retinal interneuron that delivers excitatory synaptic input to ganglion cells. Consistent with this, the electric fields arising from parallel orientation of the coil were oriented perpendicularly into the retina, the orientation thought to be optimal for bipolar cell activation. This raises the possibility that here, the inability to elicit burst responses in STN neurons, may simply reflect a lack of viable presynaptic excitatory neurons, likely resulting from preparation of the coronal slice. Suboptimum orientation of the induced electric field with respect to targeted neuronal processes may also have contributed to the lack of burst firing. Whereas retinal bipolar cells are uniformly oriented, there is considerable variability in the arrangement of pre- and post-synaptic processes within the STN and therefore considerably more variability in their alignment with induced fields.

In the retinal study, responses to μMS consisted of only a single short latency spike (~ 1 ms) when the central coil axis was rotated to be perpendicular to the retinal surface. Studies utilizing electric stimulation of the retina have consistently shown that single short latency spikes arise only from direct activation of ganglion cells [50], [52], [58], [59]. Thus, the short-latency single spike arising from μMS of the retina was likely to have arisen from direct activation as well and is consistent with induced electric fields that were oriented along the ganglion cell axon (arising from perpendicular orientation of the coil). Here however, we found single, short-latency spikes elicited by μMS in only three of seven cells that were tested. Further, the average threshold for the three cells that could be activated was 23 V, approximately 30% higher than that required for direct activation in the retinal study (17.7 V). While the phase-locked short-latency spikes observed here indicate that direct activation of STN neurons is possible, the elevated thresholds and limited success rate suggest that further optimization is required. The factors underlying the responsiveness difference (retinal versus STN) were not revealed by this study but anatomical differences between the two types of neurons may contribute. For instance, the axons of ganglion cells emerge from the soma to run along the top-most surface of the *in vitro* retinal preparation [58]. With this orientation the dense band of sodium channels within the initial segment of the proximal axon, the site known to have the highest sensitivity to electric stimulation [58], was positioned directly below the center of the μMS coil. In contrast, the axons of STN

neurons emerge down and away from the μMS coil in the coronal slices [60]–[64] utilized here. Thus the limited success for activation of STN neurons could result from the larger distance between coil and axon. It is also possible that one or more intrinsic differences between the two types of neurons also contribute to the threshold difference, e.g., differences in the properties of the sodium channel band are known to influence threshold and could be different in retinal versus STN neurons [58], [62].

In contrast to the limited and inconsistent responses elicited by single pulses of μMS, responses to repetitive μMS (r-μMS) were reliable and robust. All cells to which r-μMS was applied exhibited an increase in the level of spiking although there was variability in both the level and duration of the increase. In a small percentage of cells (n = 2/28), the increase in spiking consisted of intermittent bursts that persisted for the duration of the μMS stimulus [Fig. 5(c)]. In all other cells (n = 26/28), the spiking elicited by μMS manifested as an increase in the regular (nonbursting) rate of spiking. The level of increase ranged considerably, e.g., for some cells the spiking increase went only slightly above baseline [Fig. 5(b)] while for other cells the increase was more substantial [Fig. 4(a)]. In most cells for which an increase in regular (nonburst) spiking was observed (n = 26/28), ongoing r-μMS resulted in a complete cessation of spiking (n = 21/26).

Although our study does not reveal why some STN neurons were suppressed and some were not, it is interesting that the percentage of STN neurons suppressed by r-μMS in our study (75%) is highly similar to the percentage of cells in which spiking was suppressed by high-frequency electric stimulation (HFS) in previous studies [46]. The suppression arising from persistent stimulation in both types of studies occurred only after a period of increased spiking, raising the possibility that suppression is mediated by some sort of fatigue. This is not certain however since similar to the spiking rates elicited by electric stimulation, the rates induced by μMS remained well below the rates that are thought to arise physiologically [65] and other mechanisms have been suggested [66], [67]. The biggest difference between the responses to μMS and the responses to electric stimulation was in the latency to the onset of response suppression; in response to electric stimulation (HFS) latencies were quite short (10 – 25 seconds [46]) while here we found considerable variability (69 – 262 seconds) across cells. The reasons for this variability are not clear but they may again reflect subtle differences in the orientation of the coil relative to the targeted cell and/or other intrinsic differences across cells. Changes to the parameters of the stimulus waveform altered the latency to the onset of suppression in a predictable manner: stimuli that utilized higher levels of power were associated with shorter latencies [Fig. 7(b) and (d)]. When two different stimuli with equal power were compared, the one that was delivered more regularly had a shorter latency when compared to waveforms that delivered the identical energy but within a shorter time period [Fig. 7(e)-(f)].

μMS Is suitable as a next-generation DBS device? The mechanism(s) underlying DBS are still unresolved [67] and therefore it is difficult to point to a specific result from *in vitro* stimulation and form a definitive conclusion. Nevertheless, the fact that response patterns with μMS *in vitro* were similar to the patterns from electric stimulation seen in previous studies is encouraging. Further, the ability of μMS to both suppress (Fig. 4)] and induce (Fig. 4(a), Ref Bonmassar *et al.* [36]) neural activity suggests that a wide range of

modulatory effects may ultimately be able to be created, including the one(s) that ultimately are shown to mediate clinical responsiveness. Further, the potential to avoid activation of passing axons with μMS [36] may help reduce unwanted side effects. Thus, further study of the fundamental interactions between magnetic stimulation and neuronal activation is warranted as it will help create a foundation from which μMS can be evaluated in *in vivo* and ultimately in clinical trials. It will be especially important to learn how and why responses shift from excitatory to inhibitory.

The power levels required to supply microcoils will also be an important factor as μMS is considered as a potential alternative to existing neural prosthetic devices. In the present study, the duration of the waveform input to the coil was 20 μs for the large-amplitude leading bi-phasic element and 12 ms for the subsequent decaying sinusoid [Fig. 2(b)]. Because Faraday's Laws indicate that the strength of the induced magnetic field is proportional to the amplitude of the current waveform, the larger magnitude of the leading waveform would suggest it underlies the response to pulsatile stimulation, both here as well as in the earlier retinal study. The duration of the leading waveform (20 μs) is however considerably shorter than the time over which neurons are thought to optimally respond to artificial stimulation [68] and the portion of time for which the neuron would be significantly depolarized is even shorter. Thus, the damped sinusoid component may also contribute to activation and our results do not reveal whether one of the two components was more effective for activation than the other; the corresponding power level for each of these two components was 1.32 and 38.48 mJ (respectively), suggesting it would be more economical from a power consumption point of view if the shorter component was in fact responsible for activation. However, even at 1.32 mJ/pulse, the power necessary at stimulation rates comparable to existing HFS DBS would require power levels of close to 200 mJ for repetitive pulsatile μMS; this level is considerably higher than the range of levels (0.03 – 1.9 mJ) used by existing neural prosthetics, e.g., HFS DBS for the treatment of PD [49]. Importantly, we found strong suppression of neuronal activity with r-μMS even at very low stimulus rates. Presumably, the suppression of STN activity arising from low rate μMS will yield the same clinical benefit as the suppression of STN activity that occurs with HFS DBS and therefore the power levels associated with repetitive μMS may lie within a more reasonable range. For example, the power level associated with a single 500-Hz sinusoid delivered at 1 Hz was 2.31 mJ. While the power level for this type of r-μMS still slightly exceeds the upper limit for existing DBS, all μMS experiments to date have utilized the identical, commercially available coil (Section II). Next generation experiments will utilize new coil sizes and/or shapes that are optimized to reduce power levels even further and will bring μMS power levels much closer or possibly even below the levels used by existing devices.

In addition to power consideration, a myriad of other safety and efficacy issues will need to be evaluated before more serious consideration can be given to μMS as a clinical device. For example, the long-term biocompatibility of an implanted coil system will need to be tested. A potential advantage of μMS is that the metal coils can be coated with one or more bio-inert polymers [40]–[44] without any significant loss in efficacy; this may help to reduce the risk of inflammatory reactions. Further, the diameter of the coil used in this study (0.5 mm)

is less than one-half the diameter of existing DBS leads. A smaller diameter implant may help to further reduce the inflammatory or immune reactions associated with implantation. Before concluding that the 0.5-mm diameter is optimum however, it will be necessary to determine the spatial extent of stimulation as a function of coil diameter in order to ensure that the entire targeted region is activated appropriately. Finally, because the mechanisms underlying efficacy are still under investigation for many neural prosthetic applications, e.g., HFS DBS for PD [67], it will be necessary during *in vivo* and clinical trials to ascertain whether μMS does in fact elicit comparable clinical benefits. Although this can only be determined experimentally, our results here imply that if the ability to suppress STN neurons is key, the effectiveness of μMS may be comparable to existing devices.

Acknowledgment

D. K. Eddington provided some helpful suggestions during the initial phase of this study and E. S. Sanchez provided training with brain slice preparations.

This work was supported by the Veterans Administration under Grant MR 1I01RX000350-01A1 and by the National Eye Institute under Grant R01EY019967 and Grant R01EY023651.

Biography

Seung Woo Lee was born in Seoul, Korea, in 1979. He received the B.S. and Ph.D. degrees in electrical engineering and computer science from Seoul National University (SNU), Seoul, Korea, in 2003 and 2010, respectively. His Ph.D. degree thesis was on the development of long-term implantable neuro-prosthetic devices using Liquid Crystal Polymers.

He was a Research Fellow in the Inter-university Semiconductor Research Center (ISRC), Seoul National University, until December 2010. Since January 2011, he has been working as a Research Fellow in the Department of Neurosurgery, Massachusetts General Hospital (MGH) and Harvard Medical School, Boston, MA, USA. He is also participating in Boston Retinal Implant Project in Center for Innovative Visual Rehabilitation at Boston Veterans Administration (VA) Healthcare System, Boston, MA, USA. His research interests include

development of chronic implantable electronic system (BioMEMs and Bioelectronics) as well as effective electric/magnetic neural stimulation strategy (neurophysiology) for neuroscience research and neural prosthesis.

Shelley I. Fried was born in Brooklyn, New York City, NY, USA, in 1961. He received the B.E. degree in mechanical engineering from Cooper Union, NY, in 1982, the M.S. degree in biomedical engineering from the Pennsylvania State University in 1986 and the Ph.D. degree in vision science from the University of California, Berkeley, CA, USA, in 2004.

From 2004 to 2006, he was a Postdoctoral Fellow in the Molecular and Cell Biology Department, Berkeley, and from 2006 to 2007 he was a Research Fellow at the Massachusetts General Hospital, Department of Neurosurgery, Boston, MA, USA. Since 2008, he has been a Research Scientist at the Boston Veterans Administration Healthcare System and an Assistant in Neuroscience at the Massachusetts General Hospital. He is also an Assistant Professor in the Department of Neurosurgery, Harvard Medical School, Boston. His research interests lie within the field of neural prosthetics with a focus towards understanding the fundamental mechanisms by which neurons respond to artificial stimulation.

References

1. Benabid AL, Chabardes S, Mitrofanis J, Pollak P. Deep brain stimulation of the subthalamic nucleus for the treatment of Parkinson's disease. Lancet Neurol. Jan.2009 8:67–81. [PubMed: 19081516]
2. Wichmann T, Delong MR. Deep brain stimulation for neurologic and neuropsychiatric disorders. Neuron. Oct.2006 52:197–204. [PubMed: 17015236]
3. Kringelbach ML, Jenkinson N, Owen SL, Aziz TZ. Translational principles of deep brain stimulation. Nat. Rev. Neurosci. Aug.2007 8:623–635. [PubMed: 17637800]
4. Wilson BS, Dorman MF. Cochlear implants: Current designs and future possibilities. J. Rehabil. Res. Dev. 2008; 45:695–730. [PubMed: 18816422]
5. Wilson BS, Finley CC, Lawson DT, Wolford RD, Eddington DK, Rabinowitz WM. Better speech recognition with cochlear implants. Nature. Jul.1991 352:236–238. [PubMed: 1857418]
6. Loewenstein JI, Montezuma SR, Rizzo JF III. Outer retinal degeneration: An electronic retinal prosthesis as a treatment strategy. Arch Ophthalmol. Apr.2004 122:587–596. [PubMed: 15078678]
7. Ahuja AK, Dorn JD, Caspi A, McMahon MJ, Dagnelie G, Dacruz L, Stanga P, Humayun MS, Greenberg RJ. Blind subjects implanted with the Argus II retinal prosthesis are able to improve performance in a spatial-motor task. Br. J. Ophthalmol. Apr.2011 95:539–543. [PubMed: 20881025]
8. Wilke R, Gabel VP, Sachs H, Schmidt KUB, Gekeler F, Besch D, Szurman P, Stett A, Wilhelm B, Peters T, Harscher A, Greppmaier U, Kibbel S, Benav H, Bruckmann A, Stingl K, Kusnyerik A, Zrenner E. Spatial resolution and perception of patterns mediated by a subretinal 16-electrode array in patients blinded by hereditary retinal dystrophies. Invest. Ophthalmol. Vis. Sci. Jul.2011 52:5995–6003. [PubMed: 21693599]

9. Brindley GS, Lewin WS. The sensations produced by electrical stimulation of the visual cortex. J. Physiol. May.1968 196:479–493. [PubMed: 4871047]
10. Schmidt EM, Bak MJ, Hambrecht FT, Kufta CV, O'Rourke DK, Vallabhanath P. Feasibility of a visual prosthesis for the blind based on intracortical microstimulation of the visual cortex. Brain. Apr.1996 119(2):507–522. [PubMed: 8800945]
11. Sheffler LR, Chae J. Neuromuscular electrical stimulation in neurorehabilitation. Muscle Nerve. May.2007 35:562–590. [PubMed: 17299744]
12. Peckham PH, Knutson JS. Functional electrical stimulation for neuromuscular applications. Annu. Rev. Biomed Eng. 2005; 7:327–360. [PubMed: 16004574]
13. Visser-Vandewalle V. DBS in Tourette syndrome: Rationale, current status and future prospects. Acta. Neurochir. Suppl. 2007; 97:215–222. [PubMed: 17691307]
14. de Koning PP, Figee M, van den Munckhof P, Schuurman PR, Denys D. Current status of deep brain stimulation for obsessive-compulsive disorder: A clinical review of different targets. Curr. Psychiatry Rep. Aug.2011 13:274–282. [PubMed: 21505875]
15. Mian MK, Campos M, Sheth SA, Eskandar EN. Deep brain stimulation for obsessive-compulsive disorder: Past, present, and future. Neurosurg. Focus. Aug.2010 29:E10. [PubMed: 20672912]
16. Levy RM, Lamb S, Adams JE. Treatment of chronic pain by deep brain stimulation: Long term follow-up and review of the literature. Neurosurgery. Dec.1987 21:885–893. [PubMed: 3325851]
17. Hauptman JS, DeSalles AA, Espinoza R, Sedrak M, Ishida W. Potential surgical targets for deep brain stimulation in treatment-resistant depression. Neurosurg. Focus. 2008; 25:E3. [PubMed: 18590380]
18. Halpern CH, Samadani U, Litt B, Jaggi JL, Baltuch GH. Deep brain stimulation for epilepsy. Neurotherapeutics. Jan.2008 5:59–67. [PubMed: 18164484]
19. Deuschl G. Deep brain stimulation: Postoperative issues. Mov. Disord. 2006; 21:S219–S237. [PubMed: 16810719]
20. Hariz MI. Complications of deep brain stimulation surgery. Mov. Disord. 2002; 17:S162–S166. [PubMed: 11948772]
21. Baker KB, Montgomery EB, Rezai AR, Burgess R, Luders HO. Subthalamic nucleus deep brain stimulus evoked potentials: Physiological and therapeutic implications. Mov. Disord. 2002; 17:969–983. [PubMed: 12360546]
22. Grill WM. Temporal excitation properties of paresthesias evoked by thalamic microstimulation. Clin. Neurophysiol. 2005; 116:1227–1234. [PubMed: 15826866]
23. Butson CR, Maks CB, McIntyre CC. Sources and effects of electrode impedance during deep brain stimulation. Clin. Neurophysiol. Feb.2006 117:447–454. [PubMed: 16376143]
24. Haberler C, Alesch F, Mazal PR, Pilz P, Jellinger K, Pinter MM, Hainfellner JA, Budka H. No tissue damage by chronic deep brain stimulation in Parkinson's disease. Ann. Neurol. Sep.2000 48:372–376. [PubMed: 10976644]
25. Henderson JM, Pell M, O'Sullivan DJ, McCusker EA, Fung VS, Hedges P, Halliday GM. Postmortem analysis of bilateral subthalamic electrode implants in Parkinson's disease. Mov. Disord. Jan.2002 17:133–137. [PubMed: 11835450]
26. Moss J, Ryder T, Aziz TZ, Graeber MB, Bain PG. Electron microscopy of tissue adherent to explanted electrodes in dystonia and Parkinson's disease. Brain. Dec.2004 127:2755–2763. [PubMed: 15329356]
27. Nielsen MS, Bjarkam CR, Sorensen JC, Bojsen-Moller M, Sunde NA, Ostergaard K. Chronic subthalamic high-frequency deep brain stimulation in Parkinson's disease—A histopathological study. Eur. J. Neurol. Feb.2007 14:132–138. [PubMed: 17250719]
28. Kim YT, Hitchcock RW, Bridge MJ, Tresco PA. Chronic response of adult rat brain tissue to implants anchored to the skull. Biomaterials. 2004; 25:2229–2237. [PubMed: 14741588]
29. Polikov VS, Tresco PA, Reichert WM. Response of brain tissue to chronically implanted neural electrodes. J. Neurosci. Methods. 2005; 148:1–18. [PubMed: 16198003]
30. Barker AT, Jalinous R, Freeston IL. Non-invasive magnetic stimulation of human motor cortex. Lancet. May.1985 1:1106–1107. [PubMed: 2860322]

31. George MS, Wassermann EM, Williams WA, Callahan A, Ketter TA, Basser P, Hallett M, Post RM. Daily repetitive transcranial magnetic stimulation (rTMS) improves mood in depression. Neuroreport. Oct.1995 6:1853–1856. [PubMed: 8547583]
32. Hallett M. Transcranial magnetic stimulation and the human brain. Nature. Jul.2000 406:147–150. [PubMed: 10910346]
33. Wassermann EM, Zimmermann T. Transcranial magnetic brain stimulation: Therapeutic promises and scientific gaps. Pharmacol. Ther. Jan.2012 133:98–107. [PubMed: 21924290]
34. Kobayashi M, Pascual-Leone A. Transcranial magnetic stimulation in neurology. Lancet Neurol. Mar.2003 2:145–156. [PubMed: 12849236]
35. Wagner T, Valero-Cabre A, Pascual-Leone A. Noninvasive human brain stimulation. Annu. Rev. Biomed. Eng. 2007; 9:527–565. [PubMed: 17444810]
36. Bonmassar G, Lee SW, Freeman DK, Polasek M, Fried SI, Gale JT. Microscopic magnetic stimulation of neural tissue. Nat. Commun. 2012; 3:921. [PubMed: 22735449]
37. Tischler H, Wolfus S, Friedman A, Perel E, Pashut T, Lavidor M, Korngreen A, Yeshurun Y, Bar-Gad I. Mini-coil for magnetic stimulation in the behaving primate. J. Neurosci. Methods. Jan.2011 194:242–251. [PubMed: 20974177]
38. Rattay F. Analysis of models for external stimulation of axons. IEEE Trans. Biomed. Eng. Oct. 1986 33:974–977. [PubMed: 3770787]
39. Grumet AE, Wyatt JL Jr. Rizzo JF III. Multi-electrode stimulation and recording in the isolated retina. J. Neurosci. Methods. Aug.2000 101:31–42. [PubMed: 10967359]
40. Hsu JM, Rieth L, Normann RA, Tathireddy P, Solzbacher F. Encapsulation of an integrated neural interface device with Parylene C. IEEE Trans. Biomed. Eng. Jan.2009 56:23–29. [PubMed: 19224715]
41. Kim ET, Kim C, Lee SW, Seo JM, Chung H, Kim SJ. Feasibility of microelectrode array (MEA) based on silicone-polyimide hybrid for retina prosthesis. Invest. Ophthalmol. Vis. Sci. Sep.2009 50:4337–4341. [PubMed: 19264890]
42. Bae SH, Che JH, Seo JM, Jeong J, Kim ET, Lee SW, Koo KI, Suaning GJ, Lovell NH, Cho DI, Kim SJ, Chung H. In vitro biocompatibility of various polymer-based microelectrode arrays for retinal prosthesis. Invest. Ophthalmol. Vis. Sci. May.2012 53:2653–2657. [PubMed: 22427592]
43. Lee SW, Seo JM, Ha S, Kim ET, Chung H, Kim SJ. Development of microelectrode arrays for artificial retinal implants using liquid crystal polymers. Invest. Ophthalmol. Vis. Sci. Dec.2009 50:5859–5866. [PubMed: 19553608]
44. Lee SW, Min KS, Jeong J, Kim J, Kim SJ. Monolithic encapsulation of implantable neuroprosthetic devices using liquid crystal polymers. IEEE Trans. Biomed. Eng. 2011; 58:2255–2263.
45. Beurrier C, Bioulac B, Audin J, Hammond C. High-frequency stimulation produces a transient blockade of voltage-gated currents in subthalamic neurons. J. Neurophysiol. Apr.2001 85:1351–1356. [PubMed: 11287459]
46. Magarinos-Ascone C, Pazo JH, Macadar O, Buno W. High-frequency stimulation of the subthalamic nucleus silences subthalamic neurons: A possible cellular mechanism in Parkinson's disease. Neurosci. 2002; 115:1109–1117.
47. Garcia L, Audin J, D'Alessandro G, Bioulac B, Hammond C. Dual effect of high-frequency stimulation on subthalamic neuron activity. J. Neurosci. Sep.2003 23:8743–8751. [PubMed: 14507974]
48. McIntyre CC, Grill WM, Sherman DL, Thakor NV. Cellular effects of deep brain stimulation: Model-based analysis of activation and inhibition. J. Neurophysiol. Apr.2004 91:1457–1469. [PubMed: 14668299]
49. Kuncel AM, Grill WM. Selection of stimulus parameters for deep brain stimulation. Clin. Neurophysiol. Nov.2004 115:2431–2441. [PubMed: 15465430]
50. Cai C, Twyford P, Fried S. The response of retinal neurons to high-frequency stimulation. J. Neural. Eng. Jun.2013 10:036009. [PubMed: 23594620]
51. Lee SW, Eddington DK, Fried SI. Responses to pulsatile subretinal electric stimulation: Effects of amplitude and duration. J. Neurophysiol. Apr.2013 109:1954–1968. [PubMed: 23343891]

52. Fried SI, Hsueh HA, Werblin FS. A method for generating precise temporal patterns of retinal spiking using prosthetic stimulation. J. Neurophysiol. Feb.2006 95:970–978. [PubMed: 16236780]
53. Chan CY, Nicholson C. Modulation by applied electric fields of Purkinje and stellate cell activity in the isolated turtle cerebellum. J. Physiol. Feb.1986 371:89–114. [PubMed: 3701658]
54. Francis JT, Gluckman BJ, Schiff SJ. Sensitivity of neurons to weak electric fields. J. Neurosci. Aug.2003 23:7255–7261. [PubMed: 12917358]
55. Eickenscheidt M, Jenkner M, Thewes R, Fromherz P, Zeck G. Electrical stimulation of retinal neurons in epiretinal and subretinal configuration using a multicapacitor array. J. Neurophysiol. May.2012 107:2742–2755. [PubMed: 22357789]
56. Stett A, Barth W, Weiss S, Haemmerle H, Zrenner E. Electrical multisite stimulation of the isolated chicken retina. Vision Res. 2000; 40:1785–1795. [PubMed: 10814763]
57. Jensen RJ, Ziv OR, Rizzo JF. Responses of rabbit retinal ganglion cells to electrical stimulation with an epiretinal electrode. J. Neural. Eng. Mar.2005 2:S16–21. [PubMed: 15876650]
58. Fried SI, Lasker AC, Desai NJ, Eddington DK, Rizzo JF III. Axonal sodium-channel bands shape the response to electric stimulation in retinal ganglion cells. J. Neurophysiol. Apr.2009 101:1972–1987. [PubMed: 19193771]
59. Sekirnjak C, Hottowy P, Sher A, Dabrowski W, Litke AM, Chichilnisky EJ. High-resolution electrical stimulation of primate retina for epiretinal implant design. J. Neurosci. Apr.2008 28:4446–4456. [PubMed: 18434523]
60. Hammond C, Yelnik J. Intracellular labelling of rat subthalamic neurones with horseradish peroxidase: Computer analysis of dendrites and characterization of axon arborization. Neurosci. Apr.1983 8:781–790.
61. Rafols JA, Fox CA. The neurons in the primate subthalamic nucleus: A Golgi and electron microscopic study. J. Comp. Neurol. Jul.1976 168:75–111. [PubMed: 819471]
62. Atherton JF, Wokosin DL, Ramanathan S, Bevan MD. Autonomous initiation and propagation of action potentials in neurons of the subthalamic nucleus. J. Physiol. Dec.2008 586:5679–700. [PubMed: 18832425]
63. Bevan MD, Booth PA, Eaton SA, Bolam JP. Selective innervation of neostriatal interneurons by a subclass of neuron in the globus pallidus of the rat. J. Neurosci. Nov.1998 18:9438–9452. [PubMed: 9801382]
64. Afsharpour S. Light microscopic analysis of Golgi-impregnated rat subthalamic neurons. J. Comp. Neurol. Jun.1985 236:1–13. [PubMed: 4056088]
65. Wilson CJ, Bevan MD. Intrinsic dynamics and synaptic inputs control the activity patterns of subthalamic nucleus neurons in health and in Parkinson's disease. Neurosci. Dec.2011 198:54–68.
66. Gradinaru V, Mogri M, Thompson KR, Henderson JM, Deisseroth K. Optical deconstruction of parkinsonian neural circuitry. Science. Apr.2009 324:354–359. [PubMed: 19299587]
67. Montgomery EB Jr. Gale JT. Mechanisms of action of deep brain stimulation (DBS). Neurosci. Biobehav. Rev. 2008; 32:388–407. [PubMed: 17706780]
68. Ranck JB Jr. Which elements are excited in electrical stimulation of mammalian central nervous system: A review. Brain Res. Nov.1975 98:417–440. [PubMed: 1102064]

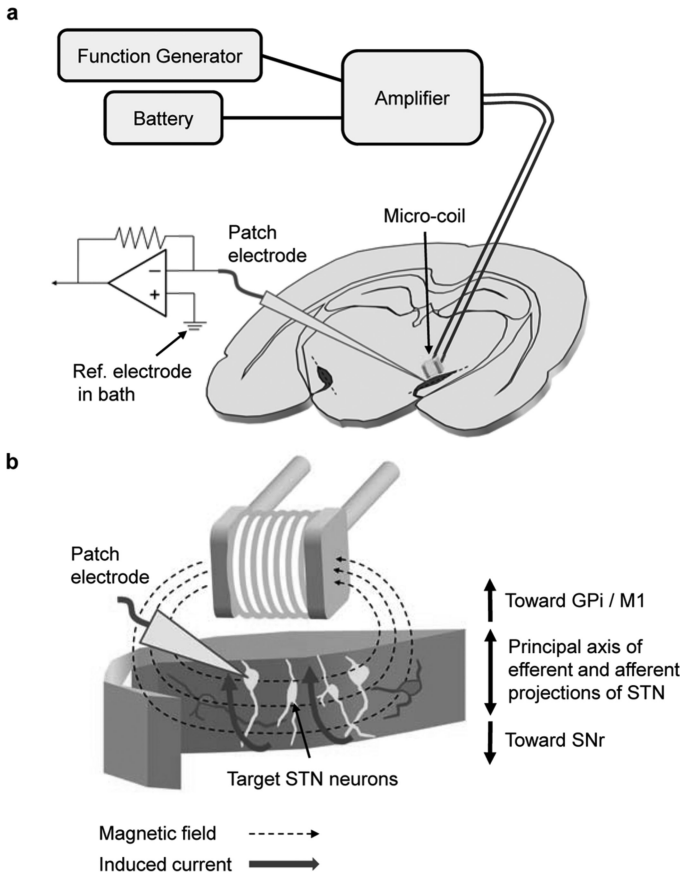

Fig. 1.

Micromagnetic stimulation (μMS) of subthalamic nucleus (STN) neurons. (a) Schematic representation of experimental setup: A patch electrode was used to record neural activity from STN neurons in response to stimulation from a microcoil; the stimulus waveform was generated by a function generator and then amplified prior to delivery of the coil. Coil was positioned 300 μm above the surface of the coronal slice and centered over the STN (dark shaded area). Central axis of the coil was held parallel to the top surface of the slice and also parallel to the long axis of the STN (dashed lines). Recording system was electrically isolated from the battery-powered magnetic stimulation system in order to avoid any direct or indirect currents between the systems. (b) Conceptual diagram illustrating the approximate orientation of the coil along with the lines of magnetic field emanating from the coil. Induced currents (solid thick arrow) were aligned with the principal axis of efferent and afferent projections of STN neurons so as to optimize targeting.

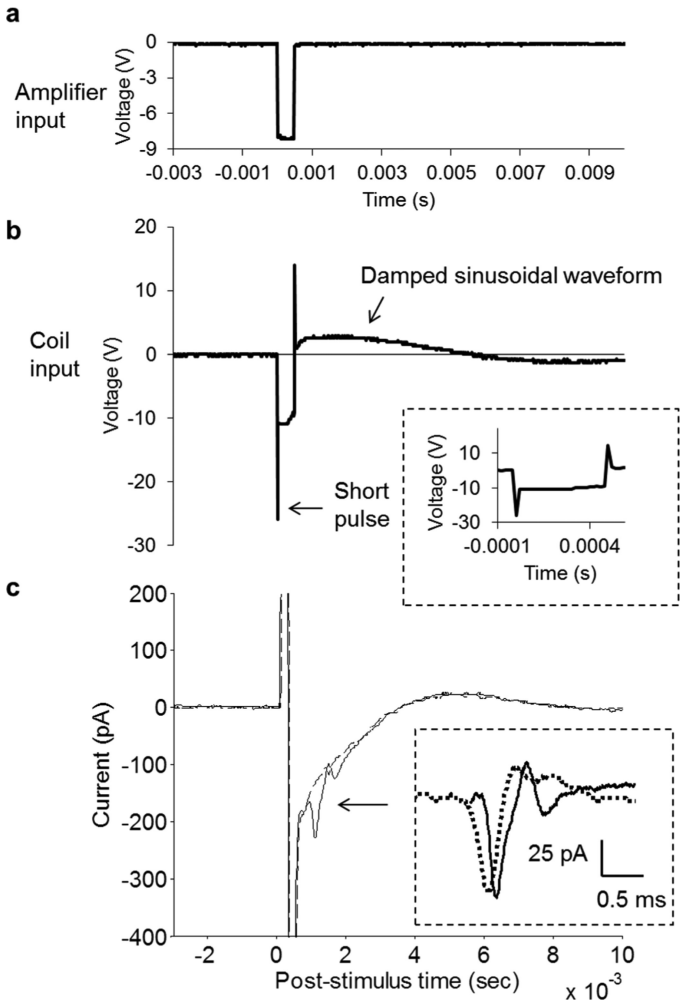

Fig. 2.

Direct activation of STN neurons by “pulsatile” stimulation. (a) Measured output of the function generator was a 500-μs pulse. (b) Amplifier transformed the pulse into a complex waveform consisting of two short durations (20 μs) bi-phasic components (inset: expanded time scale allows better visualization of negative and positive peaks separated by 500-μs interval) and a longer, damped sinusoid immediately following completion of the pulse. (c) Overlay of two trials in response to the same pulsatile stimulus; both responses were highly similar but one (solid line) contained a multiphasic waveform (arrow) starting approximately 1 ms after stimulus onset. The other response (dashed line) was otherwise identical but lacked the multiphasic waveform. (Inset) Subtraction of the two waveforms reveals a response waveform (solid line) that is highly similar to an action potential that arose spontaneously from the same cell (dotted line). Two traces are horizontally offset slightly to facilitate comparison.

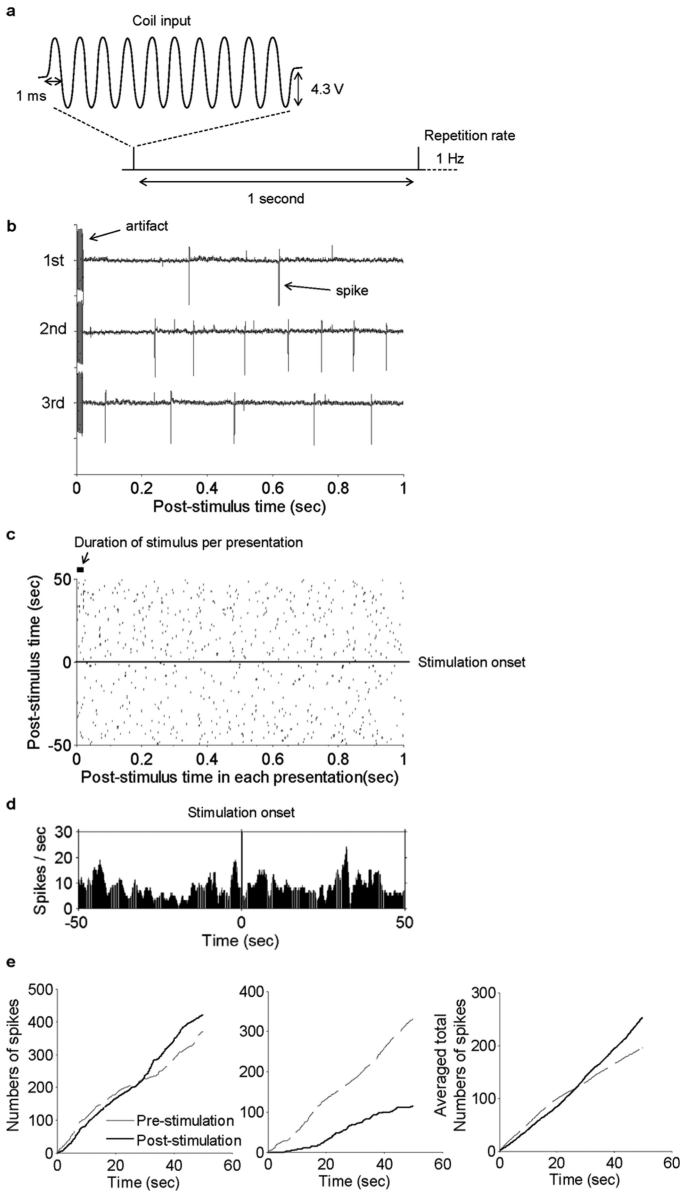

Fig. 3.

Sinusoidal μMS stimulation suppresses activity in most STN neurons. (a) Input to the coil consisted of ten cycles of a 500-Hz sinusoid with a constant amplitude of 4.3 V; this pattern of ten cycles was repeated every 1 s (1 Hz). (b) Typical recording traces that show the stimulus artifact as well as the spikes that arose during the 1-second time period following the stimulus. (c) Peri-stimulus time raster plot for 50 one-second periods pre-stimulus (below horizontal line) and 50 one-second periods post-stimulus (above line). (d) Peri-stimulus time histogram (PSTH) for all pre- and post-stimulus time periods (Binsize = 0.1 s) (e) Total spike counts versus time for pre- and post-stimulation time periods. Left panel is the cell from Panels b-d; center panel is from a different cell; right panel is the average from all cells (n = 28).

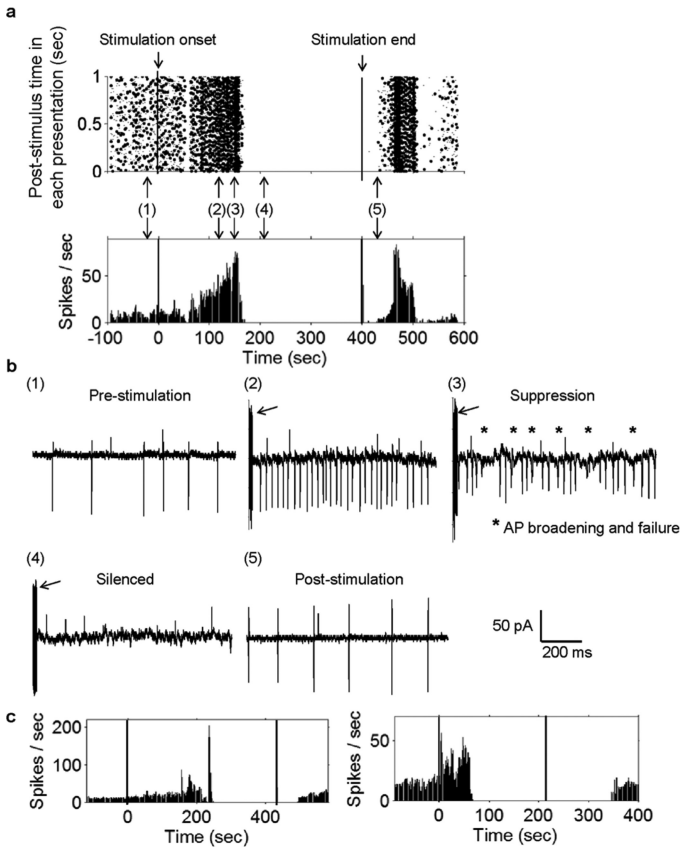

Fig. 4.

Prolonged sinusoidal μMS stimulation suppresses activity in most STN neurons. Response of a typical STN neuron to ten cycles of a 500-Hz sinusoid delivered at a repetition rate of 1 Hz. (a) Peri-stimulus raster plot from a typical cell (top); each column depicts the spikes that occurred in the one-second interval corresponding to that time. The corresponding PSTH is shown at the bottom. Left and right vertical lines indicate onset and offset of μMS (respectively). (b) Panels 1–5 reveal expanded one second snapshots of the cell's response; panels correspond to the time points indicated in (a). The arrows in Panels 2–4 point to the electrical artifact associated with the μMS stimulus. (c) Typical PSTHs from two other STN neurons that were also silenced. Note that the duration over which μMS was applied was not uniform for all cells.

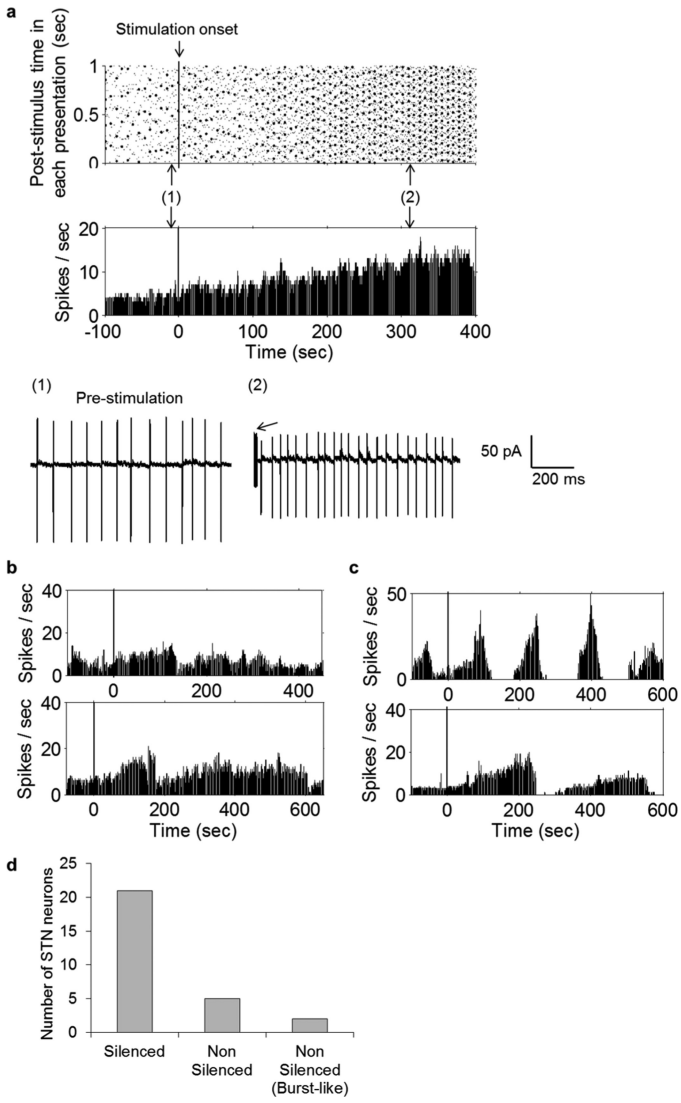

Fig. 5.

*μ*MS does not silence some STN neurons. (a) Response of an STN neuron that was not suppressed by the ten-cycle 500-Hz sinusoidal *μ*MS delivered at a repetition rate of 1 Hz. Peri-stimulus raster plot of the neuron (top) and corresponding PSTH (bottom) show that firing rate was moderately increased. Vertical line indicates the onset of *μ*MS. Panel numbers 1–2 reveal expanded one-second snapshots of the cell's response; panels correspond to the time points indicated in (a). Arrow in Panel 2 indicates the electrical artifact associated with the *μ*MS stimulus. (b) PSTHs from other two other STN neurons that were not silenced by *μ*MS. (c) PSTHs from the two neurons that showed burst-like spiking that persisted during the course of stimulation. (d) Population results showing total number of silenced (21), nonsilenced (5), and burst-like spiking (2) STN neurons.

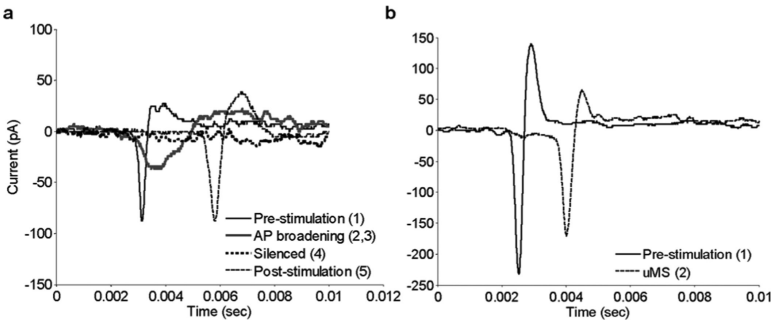

Fig. 6.

AP broadening is correlated with suppression. (a) Overlay of action potentials from different time epochs from the cell in Fig. 4(a), one example of a cell that was suppressed by μMS. Numbers in the legend correspond to the time periods (arrows) in Fig. 4(a) during which the spikes were generated. (b) Overlay of action potentials from the cell in Fig. 5(a), one example of a cell not suppressed by μMS. Numbers in legend correspond to the arrows in Fig. 5(a).

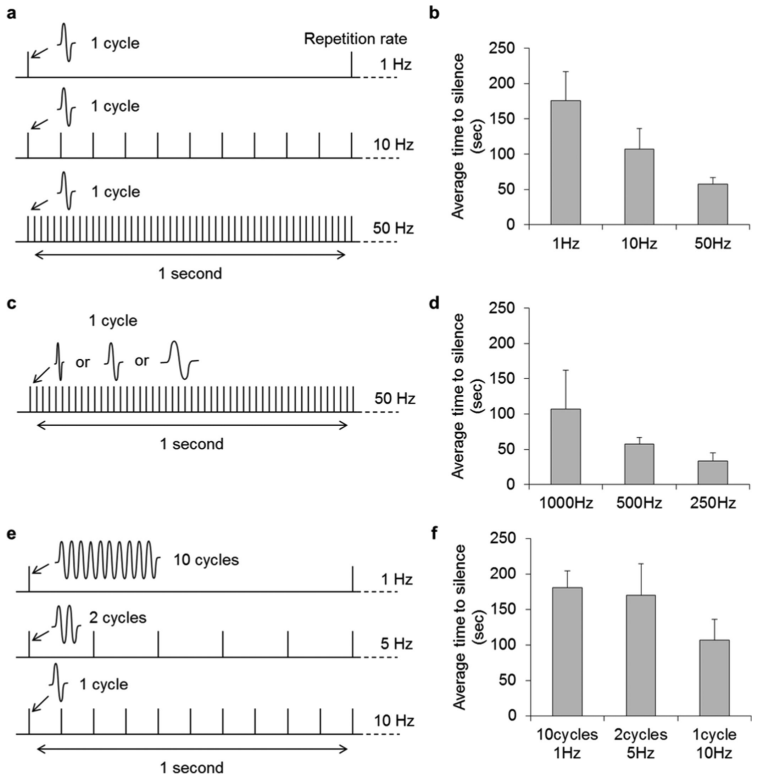

Fig. 7.

Time to silencing is stimulus-parameter dependent. (a), (b) Average time-to-silence after onset of μMS was measured for repetition rates of 1, 10, and 50 Hz; each tic mark represents a single period of a 500 Hz sinusoid. Bar graph plots the average time-to-silence for each repetition rate. (n = 10 for 1 Hz, n = 7 for 10 and 50 Hz). (c), (d) Average time-to-silence as a function of frequency of the sinusoidal waveform; each tic mark represents a single period of a 1000, 500 or 250 Hz sinusoid (n = 7). (e), (f) Average time-to-silence for three configurations each delivering ten cycles/second (n = 17 for ten cycles at 1 Hz, n = 7 for the two other configurations); each tic mark represents one (top), two (middle) or ten (bottom) periods of a 500-Hz sinusoid. Bars in b, d and f represent standard error.

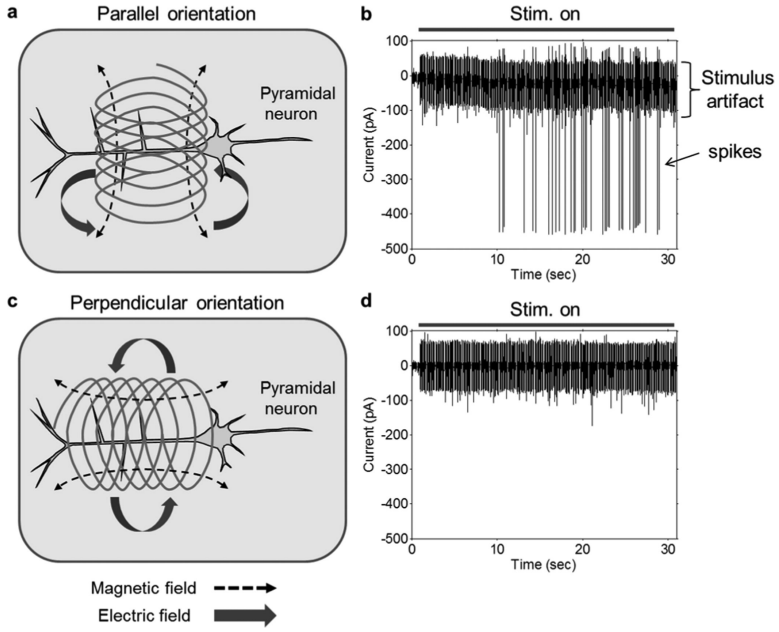

Fig. 8.

Stimulation effectiveness depends on coil orientation. (a) Parallel orientation: Central axis of the coil was parallel to the slice surface and perpendicular to the principal axis of the pyramidal neuron. Induced electric fields (solid thick arrows) were oriented along the principal axis of targeted neurons. (b) Typical response to parallel orientation stimulation consisting of elicited spikes. (c) Perpendicular orientation: Central axis of the coil was parallel to the slice surface and parallel to the principal axis of the pyramidal neuron. Induced electric fields (solid thick arrows) were oriented orthogonal to the principal axis of targeted neurons. (d) Typical neural response to the perpendicular orientation stimulation.